

Magic sizes enable minimal-complexity, high-fidelity assembly of programmable shells

Botond Tyukodi,^{1,2,3} Daichi Hayakawa,³ Douglas M. Hall,⁴ W. Benjamin Rogers,³ Gregory M. Grason,^{4,*} and Michael F. Hagan^{3,†}

¹*Department of Physics, Babeş-Bolyai University, 400084 Cluj-Napoca, Romania*

²*Centre International de Formation et de Recherche Avancées en Physique, 077125 Bucharest-Măgurele, Romania*

³*Martin Fisher School of Physics, Brandeis University, Waltham, Massachusetts 02454, USA*

⁴*Department of Polymer Science and Engineering, University of Massachusetts, Amherst, Massachusetts 01003, USA*

(Dated: November 7, 2024)

Recent advances in synthetic methods enable designing subunits that self-assemble into structures with well-defined sizes and architectures, but yields are frequently suppressed by the formation of off-target metastable structures. Increasing the complexity (number of distinct inter-subunit interaction types) can inhibit off-target structures, but leads to slower kinetics and higher synthesis costs. Here, we use icosahedral shells formed of programmable triangular subunits as a model system, and identify design principles that produce the highest target yield at the lowest complexity. We use a symmetry-based construction to create a range of design complexities, starting from the maximal symmetry Caspar-Klug assembly up to the fully addressable, zero-symmetry assembly. Kinetic Monte Carlo simulations reveal that the most prominent defects leading to off-target assemblies are a class of disclinations. We derive symmetry-based rules for identifying the optimal (lowest-complexity, highest-symmetry) design that inhibits these disclinations, leading to robust, high-fidelity assembly of targets with arbitrarily large sizes. Optimal complexity varies non-monotonically with target size, with ‘magic’ sizes appearing for high-symmetry designs in which symmetry axes do not intersect vertices of the triangular net. The optimal designs at magic sizes require 12 times fewer inequivalent interaction-types than the (minimal symmetry) fully addressable construction.

The self-limiting assembly of subunits into structures with well-defined sizes and architectures underlies the essential functions and construction of cells and the pathogens that infect them, from virus capsids [1–8] and bacterial microcompartments [9–14] to cellular protein shells [15–18]). Recent advances in DNA origami, protein design, supramolecular assembly, and patchy-colloidal particles have enabled designing synthetic subunits that undergo self-limited assembly into complex architectures, such as quasi-spherical shells and cylindrical tubes with programmable sizes [19–36]. Many of these [20, 21, 24, 28, 29, 31, 32, 35] invoke the symmetry principles of icosahedral shells identified from natural virus structures [37–40], the *Caspar-Klug* (CK) construction [41]. CK identifies the T -number as the minimal number of inequivalent subunits (i.e., different protein sequences or conformations) required to form an icosahedral shell with a particular diameter. CK thus provides a solution to the generic problem of maximizing the assembly ‘economy’ — i.e. minimizing the complexity (number of distinct species) required to assemble a specific target size, seemingly providing a ‘blueprint’ for new biomimetic synthetic assembly strategies.

Despite these spectacular successes, the ‘fidelity’ (the yield of the target structure) falls dramatically with increasing target size because thermal fluctuations of the subunit-subunit angles within the growing assemblage lead to competing off-pathway structures [8, 21]. Sim-

ilarly, Ref. [42] reported that low complexity designs (in which subunits attach irreversibly and form only pentameric or hexameric vertices) could not assemble shells with $T > 4$ without a scaffold. Fluctuations can be decreased by increasing the geometric specificity of subunit-subunit interactions, i.e., the relative cost of binding with off-target angles and distances [43, 44]. Subsequent works [25, 45–47] suggest that yields can be enhanced by further increasing the number of species (complexity) to make off-pathway structures inaccessible. However, increasing the specificity or number of species increases synthesis costs and assembly timescales [25, 48, 49], and thus becomes impractical for large targets. Existing algorithms to identify optimal designs for icosahedral shells do not a-priori account for defects that form during assembly dynamics [50–60].

This competition between assembly economy and fidelity is a generic feature of self-assembly. A major design challenge is to identify an optimal balance between the maximal design economy (a single subunit species, e.g. [7, 8, 61–77]) and perfect specificity (i.e. a fully ‘addressable’ assembly in which every subunit is a distinct species with a unique ‘address’ in the target [78–85]). In this letter, we study icosahedral shells as a model system to identify the principles that underlie a ‘Pareto optimal’ set of target structures that achieve high fidelity at the minimal possible design complexity. The principles derive from symmetry rules for obstructing disclinations, the most prominent class of defects that facilitate off-pathway assembly. Remarkably, in contrast to lower complexity designs (Ref. [42]), the optimal complexity designs achieve high-fidelity assembly of large shells

* grason@umass.edu

† hagan@brandeis.edu

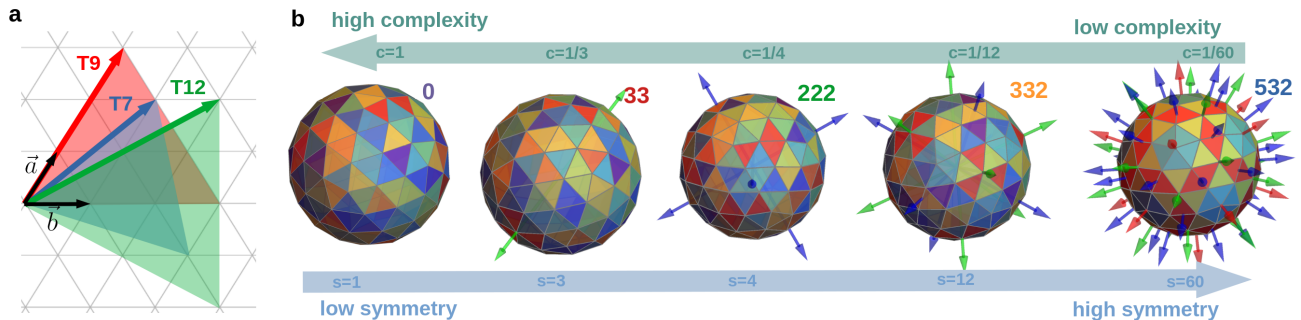


FIG. 1. (a) Construction of icosahedron facets of increasing size (T number). (b) Sequence of $T=9$ programmable shells, from left to right showing progressively *increasing symmetry* ($s = N_{\text{operations}}$) and correspondingly *decreasing complexity* ($c = N_{\text{edge-types}}/T$). Structures are labeled according to their orbifold symmetry denoting the nature of rotational symmetries in the structure (see SI section III). For clarity, we illustrate the 5-fold (red), 3-fold (green), and 2-fold (blue) rotational symmetries.

without a scaffold (500 or more subunits, limited only by our computational power, Fig. 2b and SI Fig. 3).

Designing icosahedral shells from low complexity to fully addressable. We choose triangular subunits for our model icosahedra, motivated by recent experiments in which triangular DNA origami subunits assemble into icosahedral shells or tubules[21, 23, 25, 86] and natural viruses whose capsids assemble from protein trimers (e.g. [87]). We obtain a series of icosahedra with increasing sizes by the standard CK construction of subdividing each of the 20 facets of the base icosahedron. Connecting any two points of a triangular lattice gives an edge of a base facet of desired size; repeating this base facet constructs the whole icosahedron (Fig. 1a). The base edge vector is given by $\mathbf{T} = h\mathbf{a} + k\mathbf{b}$ where \mathbf{a}, \mathbf{b} are the lattice base vectors with lengths in units of the triangular lattice spacing l_0 and h, k are integers. The number of triangles in a base facet is $T = |\mathbf{T}| = h^2 + k^2 + hk$.

Icosahedra feature three kinds of rotational symmetry axes (we do not consider mirror symmetry): 2-fold, 3-fold, and 5-fold axes on the base edges, facet centers, and base vertices respectively. CK assigns the same species for subunits in equivalent local symmetry environments, resulting in $\lceil T/3 \rceil$ species and T distinct edge-types for triangular subunits (where each edge corresponds to an individual protein in the CK construction). The preferred edge-lengths and inter-triangle dihedral angles must be slightly adjusted away from equilateral to avoid elastic costs of geometric frustration (see SI section VIII). Although we focus on icosahedra assembled from triangular subunits, our results will be qualitatively similar for other subunit shapes when adapted for the topology of their tiling in spherical nets. However, icosahedral nets encode the greatest number sub-group symmetries of any such net, enabling the widest range of ‘variable complexity’ shell designs.

To investigate how assembly depends on complexity and symmetry, we construct designs that systematically vary between the minimal complexity needed to avoid ge-

ometric frustration (i.e. CK rules) and the fully addressable case. Adopting the orbifold notation for spherical symmetry patterns [88], we start with the fully addressable 0 pattern, which has no symmetries as all triangles are distinct. Then we consider assemblies with a subset of the full symmetries of the icosahedron, corresponding to subgroup combinations of 5-, 3- and 2-fold axes. Fig. 1b shows a sequence of increasing symmetry for $T=9$ nets: 0 (fully addressable), 33, 222, 332 and 532 (CK) (see SI section III for the remaining 22, 55, 322 and 522 symmetries).

Including symmetry axes reduces the number of distinct species compared to the fully addressable 0 structures, since operating the rotational symmetry elements on the structure maps equivalent triangles (and edges) onto their multiple locations (or ‘addresses’) in the assembly. Hence, increasing the number of symmetries in a design increases the copy number of a particular triangle (subunit species) in the target structure, i.e., decreases the number of distinct subunit- and edge-types in the target structure, making it less complex. We define *complexity* as the number of distinct edge-types normalized by T : $c = N_{\text{edge-types}}/T$ (Fig. 1b). Similarly, we quantify symmetry $s = N_{\text{operations}}$ as the number of symmetry operations for which facets are equivalent.

Results. To investigate the assembly dynamics, we perform kinetic Monte Carlo (KMC) simulations using a model adapted from previous works [22, 42, 61–64, 89–93] (Fig. 2a). We represent growing shells as harmonic elastic sheets, within which subunits are triangles with spring constant ϵ_s along each edge. Each subunit has a species (distinguished by color in snapshots) and each edge has an edge-type. Edges that are complementary according to the target designs bind to each other with affinity ϵ_b , and non-complementary edges cannot bind. The ground-state curvature is programmed by a preferred dihedral angle θ_0 between adjacent face normals, with a harmonic penalty for angular deviations $0.5\kappa_b(\theta - \theta_0)^2$ with bending modulus κ_b . The bending and edge stretching moduli

define the *geometric specificity* of inter-subunit binding, i.e., the relative cost of binding with off-target angles and distances (Fig. 2a.). We perform grand canonical Monte Carlo simulations of a single shell growing in the presence of a reservoir of free subunits at constant chemical potentials, set to maintain concentrations of species c_i in the reservoir that reflect their stoichiometries in the target shell, while keeping the mean concentration $\bar{c} = \sum_{i=1}^{N_{\text{species}}} c_i / N_{\text{species}}$ the same for all designs. Further model details are in Refs. [90, 91] and SI sections V-VIII. For all results in the main text, we set the stretching modulus near the rigid limit, $\epsilon_s = 300k_B T / l_0^2$; the binding affinity to $\epsilon_b = -7k_B T$ to enable nucleation but maintain reversible assembly, and the mean concentration $\bar{c} = 6.7 \times 10^{-3} l_0^{-3}$.

We performed simulations for sizes from $T=1-16$ over a range of geometric specificity (bending modulus κ_b) values. Fig. 2 shows typical trajectories of three designs for a $T=9$ target at moderate geometric specificity $\kappa_b = k_B T / 2$. We observe that 222 assembles on-pathway and closes into the $T=9$ target, notwithstanding bending fluctuations (Fig. 2a). In contrast, the 332 and 532 (CK) designs fail, by closing at structures that are smaller than the target (Fig. 2c,d).

The predominant mechanism for misassembly is the formation of a generalization of disclination defects that form around symmetric vertices. As in standard disclinations in crystals [94], these are defects where the preferred p -fold symmetry of vertex is disrupted, for example by closing with $p \pm 1$ triangles around a given vertex, as shown schematically in Fig. 2e for 5- and 3-fold axes of the 532 structures.

Our simulations show that designs that inhibit formation of disclinations lead to remarkably robust high-fidelity assembly. Fig. 3a shows the yield (the fraction of nucleated trajectories that result in the target structure) for each design of a $T=9$ target structure as a function of κ_b . Above a threshold $\kappa_b^* \approx 1 - 10k_B T$, we observe near 100% yields for all designs because the high bending modulus prohibits disclinations. However, below this threshold the yields for the 532 and then 332 and 33 fall to nearly 0, while 222 and 0 (fully addressable) remain high even at $\kappa_b = 0.05k_B T$. Except near κ_b^* , the yields are nearly independent of κ_b . The yields decrease mainly due to closed, but off-target, non-icosahedral structures facilitated by disclinations at p -vertices (we mostly observe ‘‘preclosure’’ to lower-coordinated vertices than target values).

Notably, the symmetry order does not solely determine fidelity; the locations of the symmetry axes are crucial. For example, while 222 has lower complexity than 33, 222 performs nearly as well as the fully addressable design, 0, but 33 performs nearly as poorly as the minimal complexity CK design, 532. This performance inversion can be explained by the location of the points of rotational symmetry relative to triangular units. Although 222 has higher symmetry (and correspondingly lower complexity) than 33, its symmetry axes only cross

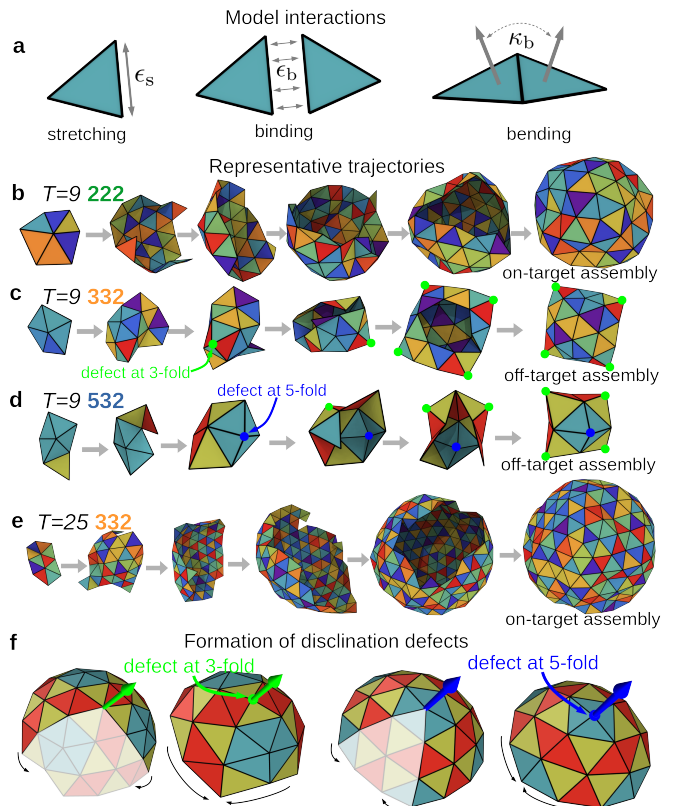


FIG. 2. (a) Subunit edges have a stretching modulus ϵ_s , complementary edges bind with affinity ϵ_b , and adjacent faces have a preferred dihedral angle θ_0 , and a harmonic bending energy modulus κ_b . (b-d) Snapshots from trajectories for a $T=9$ target with $\kappa_b = k_B T / 2$ and $\theta_0 = 0.234$ for the designs: (a) 222, (b) 332, (c) 532 (CK). Only the 222 design assembles successfully. The 332 is driven off-pathway by the formation of $+2\pi/3$ disclinations around the 3-fold symmetry axis. The 532 design mis-assembles due to $+2\pi/3$ disclinations around the 3-fold axis and either $+2\pi/5$ or $+4\pi/5$ disclinations around the 5-fold axis. (d) Snapshots from on on-target assembly trajectory for $T=25$ with $\kappa_b = k_B T$ and $\theta_0 = 0.134$ for the 332 design. (f) The Volterra construction illustrating possible disclinations at a p -fold site, visualized by the removal of a wedge of angle $2\pi/p$ (highlighted in white) and reclosing around along compatible edges, distorting according to black arrows.

subunit edges where disclinations cannot form. In contrast, the 33 3-fold symmetry axes cross through hexameric vertices where disclinations are possible (i.e. by addition/removal of $2\pi/3$ wedges). Thus, while rotational symmetries increase design economy, they can also induce the formation of off-target assemblies if those points are coincident vertices in the target net [90]. In support of this, the threshold specificity κ_b^* increases with the number of possible disclination points (see Fig. 3a and SI Fig. 9).

To further understand the interplay between complexity, symmetry, and target yields, Fig. 3b shows the yields

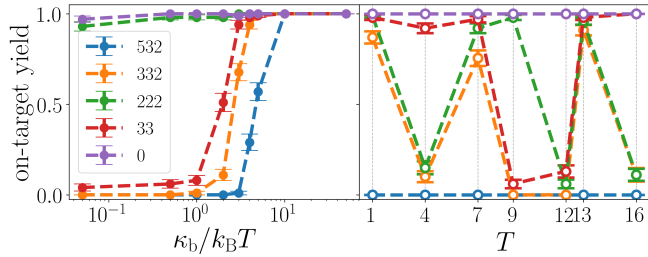


FIG. 3. (a) Yields of $T=9$ targets for the five designs as a function of bending modulus κ_b (geometric specificity). (b) Yields of each design as a function of shell size for $\kappa_b = k_B T/2$. Yields were computed from 100 independent simulations at each parameter set. Error bars are smaller than the symbol size for many points.

for each design as a function of T . As expected, the fully addressable design 0 always gives the highest yield. However, at most (but not all) T -numbers, one or more lower complexity designs perform nearly as well. We define the *optimal complexity* as the lowest complexity design that results in a yield of $\geq 75\%$. Notably, the optimal complexity varies non-monotonically with target size and, as for $T=9$, larger complexity is not necessarily better. 332 is optimal for $T=1, 7, 13$; 222 for $T=9$; 33 for $T=4$; but for $T=12$ the fully addressable design is optimal. The CK design is suboptimal for all sizes and always gives ≈ 0 yield for $\kappa_b < \kappa_b^*$.

The nonmonotonic dependency of the yield on the complexity and target size can be understood from the orientation of the symmetry axes with respect to the shell vertices. Fig. 4(a-b) show the symmetry axes of $T=7$ and $T=9$ for the 332 design. While the 2-fold axes cross edges in both designs, the 3-fold axes cross *facets* (i.e., subunit centers) for $T=7$ and *vertices* for $T=9$. This key difference allows disclinations to readily form at vertices during assembly of $T=9$, but not for $T=7$. Following this reasoning, we hypothesize that *the optimal complexity corresponds to the lowest complexity (highest symmetry) design that does not have symmetry axes crossing a vertex*. For example, for $T=7$, all of 0, 33, 22, and 332 have no symmetry axes crossing vertices and exhibit robust assembly, so 332 is the optimal complexity. For $T=9$, only 0 and 222 lack symmetry axes crossing vertices, so 222 is the optimal complexity. Since 5-fold axes necessarily cross through pentameric vertices, any design with a 5-fold symmetry axis allows disclinations for all T . This feature explains why the CK (532) and 55 designs always exhibit low yields for low κ_b .

Magic T numbers. The optimal complexity design can be predicted from geometric considerations: whenever $(2h+k)/3 \in \mathbb{Z}$ and $(k-h)/3 \in \mathbb{Z}$, the 3-fold axes cross at vertices, allowing $\pm 2\pi/3$ defects. Similarly, whenever $h/2 \in \mathbb{Z}$ and $k/2 \in \mathbb{Z}$, the 2-fold axes cross a vertex, allowing $\pm\pi$ defects. Thus, T -numbers at which both these conditions are satisfied allow disclinations if they

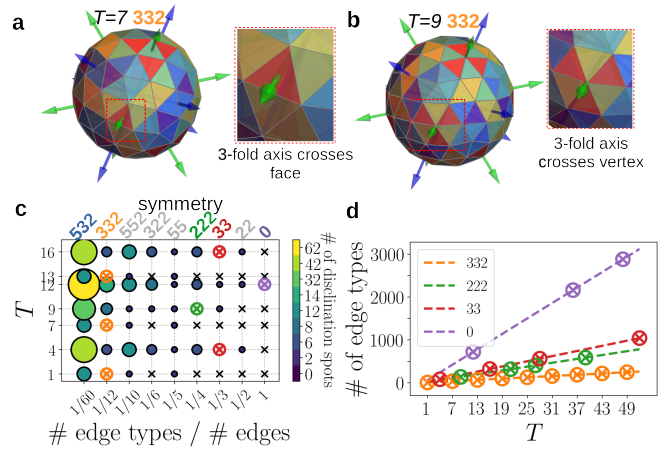


FIG. 4. Magic T numbers enable extremely economic high-fidelity assembly. (a-b) Locations of the 3-fold symmetry axes for the 332 designs with $T=7$ and $T=9$. For $T=7$ the 3-fold axis (in green) crosses through a *facet* (red), corresponding to the subunit center, and thus does not allow for disclinations. For $T=9$ the 3-fold axis crosses through a hexameric *vertex*, which allows disclinations. (c) The number of disclination points (locations where a symmetry axis crosses a vertex) for indicated complexities and T . Markers are colored and sized by the number of disclination points, and for each T number the ‘x’ symbol marks the optimal complexity at which no disclination points remain. Magic T numbers correspond to sizes at which the 2-fold and two 3-fold symmetry axes all cross through facets for the lowest complexity design without a 5-fold axis, 332. (d) The number of distinct edge-types for the optimal complexity design as a function of shell size. The dashed lines show the upper- and lower-bounds, in which the optimal design corresponds to 332 or 0 respectively. The x-axis labels show the magic T -numbers.

possess any 2-, 3- or 5-fold symmetries, and the fully addressable design will be optimal. Sizes that satisfy one condition will have an intermediate optimal complexity. Sizes that satisfy neither condition correspond to the *magic T -numbers*, which assemble robustly at any complexity that does not include a symmetric 5-fold axis (Fig. 4c and SI Fig. 4). The periodicity of these conditions gives rise to a pattern of optimal complexities ranging between 332 and 0, and a series of magic T -numbers, $\{T_{\text{magic}} = 1 + 6n \mid n \in \mathbb{Z}\}$. Fig. 4c illustrates the number of distinct edge-types required for the optimal complexity design as a function of shell size. The lower bound corresponds to the magic T -numbers, where the 332 designs assemble robustly with 12 times fewer edge-types than the fully addressable case.

Conclusions. We have demonstrated principles to identify the minimal complexity subunit design that achieves high-fidelity assembly of icosahedral shells with arbitrarily large target sizes. The designs inhibit formation of the primary class of defects that facilitate off-pathway assembly — disclinations at p -vertices — and thereby account for kinetics as well as thermody-

namics to maximize yields. Any design, including the fully addressable case, requires moderate binding affinities and subunit concentrations to avoid kinetic traps [7, 43, 44, 49, 62, 66, 95–108]. However, the optimal designs achieve nearly 100% yields over a broad range of parameter values, even for vanishing geometric specificity ($\kappa_b \lesssim 0.05k_B T$). Furthermore, for sub-optimal designs, the threshold specificity κ_b^* required for high yields increases with the number of possible disclination points. While the class of defects we identify is relevant for icosahedral shells, the same principles can be applied to nets with other symmetry elements (e.g. including 4-fold rotations).

Finally, recent advances in DNA origami [21] and protein design [32] have enabled assembly of CK shells up to $T = 100$, but with low or unmeasured yields. We anticipate that applying our design principles to these technologies can enable high-fidelity assembly of icosahedra and a wide variety of other geometries with precisely controlled sizes and architectures. Moreover, the ability of optimal designs to assemble at low geometric specificity will enable a broad array of synthesis techniques with less precision than DNA origami and protein engineering.

The data files and code used to generate the results will be publicly distributed at the time of publication.

ACKNOWLEDGMENTS

This work was supported by the NSF through DMR 2309635 (MFH, BT) and the Brandeis Center for Bioinspired Soft Materials, an NSF MRSEC (DMR-2011846) (MFH, DH, WBR, BT, DMH, GMG). This project has received funding from the European Union’s Horizon 2020 research and innovation programme under the Marie Skłodowska-Curie grant agreement No 01026118 and PNR-R-I8/C9-CF105 under contract 760099 from the Romanian Ministry of Research, Innovation, and Digitization (BT). Computing resources were provided by the National Energy Research Scientific Computing Center (NERSC), a Department of Energy Office of Science User Facility (award BES-ERCAP0026774); the NSF XSEDE allocation TG-MCB090163 (Expanse and Anvil); and the Brandeis HPCC which is partially supported by the NSF through DMR-MRSEC 2011846 and OAC-1920147.

-
- [1] Adam Zlotnick and Suchetana Mukhopadhyay. Virus assembly, allostery and antivirals. *Trends in Microbiology*, 19(1):14–23, 2011.
 - [2] Mauricio G. Mateu. Assembly, stability and dynamics of virus capsids. *Archives of Biochemistry and Biophysics*, 531(1-2):65–79, 2013.
 - [3] Robijn F. Bruinsma and William S. Klug. Physics of viral shells. *Annual Review of Condensed Matter Physics*, 6(1):245–268, 2015.
 - [4] Jason D. Perlmutter and Michael F. Hagan. Mechanisms of virus assembly. *Annual Review of Physical Chemistry*, 66:217–239, 2015.
 - [5] Michael F. Hagan and Roya Zandi. Recent advances in coarse-grained modeling of virus assembly. *Current Opinion in Virology*, 18:36–43, 2016.
 - [6] Reidun Twarock, Richard J. Bingham, Eric C. Dykeman, and Peter G. Stockley. A modelling paradigm for RNA virus assembly. *Current Opinion in Virology*, 31(Figure 1):74–81, 2018.
 - [7] Roya Zandi, Bogdan Dragnea, Alex Travesset, and Rudolf Podgornik. On virus growth and form. *Physics Reports*, 847:1–102, 2020.
 - [8] Michael F. Hagan and Gregory M. Grason. Equilibrium mechanisms of self-limiting assembly. *Reviews of Modern Physics*, 93(2):25008, 2021.
 - [9] Michael F. Schmid, Angel M. Paredes, Htet A. Khant, Ferda Soyer, Henry C. Aldrich, Wah Chiu, and Jessup M. Shively. Structure of *Halothiobacillus neapolitanus* Carboxysomes by Cryo-electron Tomography. *Journal of Molecular Biology*, 364(3):526–535, 2006.
 - [10] Cristina V. Iancu, H. Jane Ding, Dylan M. Morris, D. Prabha Dias, Arlene D. Gonzales, Anthony Martino, and Grant J. Jensen. The Structure of Isolated *Synechococcus* Strain WH8102 Carboxysomes as Revealed by Electron Cryotomography. *Journal of Molecular Biology*, 372(3):764–773, 2007.
 - [11] Cheryl A. Kerfeld, Sabine Heinhorst, and Gordon C. Cannon. Bacterial microcompartments. *Annual Review of Microbiology*, 64:391–408, 2010.
 - [12] Benjamin D. Rae, Benedict M. Long, Murray R. Badger, and G. Dean Price. Functions, Compositions, and Evolution of the Two Types of Carboxysomes: Polyhedral Microcompartments That Facilitate CO₂ Fixation in Cyanobacteria and Some Proteobacteria. *Microbiology and Molecular Biology Reviews*, 77(3):357–379, 2013.
 - [13] Chiranjit Chowdhury, Sharmistha Sinha, Sunny Chun, Todd O. Yeates, and Thomas A. Bobik. Diverse Bacterial Microcompartment Organelles. *Microbiology and Molecular Biology Reviews*, 78(3):438–468, 2014.
 - [14] Cheryl A. Kerfeld and Matthew R. Melnicki. Assembly, function and evolution of cyanobacterial carboxysomes. *Current Opinion in Plant Biology*, 31:66–75, 2016.
 - [15] Markus Sutter, Daniel Boehringer, Sascha Gutmann, Susanne Günther, David Prangishvili, Martin J. Loessner, Karl O. Stetter, Eilika Weber-Ban, and Nenad Ban. Structural basis of enzyme encapsulation into a bacterial nanocompartment. *Nature Structural and Molecular Biology*, 15(9):939–947, 2008.
 - [16] Felicitas Pfeifer. Distribution, formation and regulation of gas vesicles. *Nature Reviews Microbiology*, 10(10):705–715, 2012.
 - [17] Timothy J. Nott, Evangelia Petsalaki, Patrick Farber, Dylan Jervis, Eden Fussner, Anne Plochowitz, Timothy D. Craggs, David P. Bazett-Jones, Tony Pawson, Julie D. Forman-Kay, and Andrew J. Baldwin. Phase Transition of a Disordered Nuage Protein Generates Environmentally Responsive Membraneless Organelles.

- Molecular Cell*, 57(5):936–947, 2015.
- [18] Boris Y. Zaslavsky, Luisa A. Ferreira, April L. Darling, and Vladimir N. Uversky. The solvent side of proteinaceous membrane-less organelles in light of aqueous two-phase systems. *International Journal of Biological Macromolecules*, 117:1224–1251, 2018.
- [19] Paul W. K. Rothmund, Axel Ekani-Nkodo, Nick Papadakis, Ashish Kumar, Deborah Kuchnir Fygenon, and Erik Winfree. Design and Characterization of Programmable DNA Nanotubes. *Journal of the American Chemical Society*, 126(50):16344–16352, dec 2004.
- [20] Erik Benson, Abdulmelik Mohammed, Johan Gardell, Sergej Masich, Eugen Czeizler, Pekka Orponen, and Björn Högberg. DNA rendering of polyhedral meshes at the nanoscale. *Nature*, 523(7561):441–444, jul 2015.
- [21] Christian Sigl, Elena M. Willner, Wouter Engelen, Jessica A. Kretzmann, Ken Sachenbacher, Anna Liedl, Fenna Kolbe, Florian Wilsch, S. Ali Aghvami, Ulrike Protzer, Michael F. Hagan, Seth Fraden, and Hendrik Dietz. Programmable icosahedral shell system for virus trapping. *Nature Materials*, 2021.
- [22] Thomas E Videbæk, Huang Fang, Daichi Hayakawa, Botond Tyukodi, Michael F Hagan, and W Benjamin Rogers. Tiling a tubule: How increasing complexity improves the yield of self-limited assembly. *Journal of Physics: Condensed Matter*, 34(13):134003, 2022.
- [23] Daichi Hayakawa, Thomas E Videbæk, Douglas M Hall, Huang Fang, Christian Sigl, Elija Feigl, Hendrik Dietz, Seth Fraden, Michael F Hagan, Gregory M Grason, et al. Geometrically programmed self-limited assembly of tubules using DNA origami colloids. *Proceedings of the National Academy of Sciences*, 119(43):e2207902119, 2022.
- [24] Wei-Shao Wei, Anthony Trubiano, Christian Sigl, Stefan Paquay, Hendrik Dietz, Michael F. Hagan, and Seth Fraden. Hierarchical assembly is more robust than egalitarian assembly in synthetic capsids. *Proceedings of the National Academy of Sciences*, 121(7), February 2024.
- [25] Thomas E Videbæk, Daichi Hayakawa, Gregory M Grason, Michael F Hagan, Seth Fraden, and W Benjamin Rogers. Economical routes to size-specific assembly of self-closing structures. *Science advances*, 10(27):eado5979, 2024.
- [26] Klaus F. Wagenbauer, Christian Sigl, and Hendrik Dietz. Gigadalton-scale shape-programmable DNA assemblies. *Nature*, 552(7683):78–83, 2017.
- [27] Robby Divine, Ha V. Dang, George Ueda, Jorge A. Fallas, Ivan Vulovic, William Sheffler, Shally Saini, Yan Ting Zhao, Infencia Xavier Raj, Peter A. Morawski, Madeleine F. Jennewein, Leah J. Homad, Yu Hsin Wan, Marti R. Tooley, Franziska Seeger, Ali Etemadi, Mitchell L. Fahning, James Lazarovits, Alex Roederer, Alexandra C. Walls, Lance Stewart, Mohammadali Mazloomi, Neil P. King, Daniel J. Campbell, Andrew T. McGuire, Leonidas Stamatatos, Hannele Ruohola-Baker, Julie Mathieu, David Veessler, and David Baker. Designed proteins assemble antibodies into modular nanocages. *Science*, 372(6537), 2021.
- [28] Gabriel L. Butterfield, Marc J. Lajoie, Heather H. Gustafson, Drew L. Sellers, Una Nattermann, Daniel Ellis, Jacob B. Bale, Sharon Ke, Garreck H. Lenz, Angelica Yehdego, Rashmi Ravichandran, Suzie H. Pun, Neil P. King, and David Baker. Evolution of a designed protein assembly encapsulating its own RNA genome. *Nature*, 552(7685):415–420, 2017.
- [29] Jacob B. Bale, Shane Gonen, Yuxi Liu, William Sheffler, Daniel Ellis, Chantz Thomas, Duilio Cascio, Todd O. Yeates, Tamir Gonen, Neil P. King, and David Baker. Accurate design of megadalton-scale two-component icosahedral protein complexes. *Science*, 353(6297):389–394, 2016.
- [30] Y. Hsia, J. B. Bale, S. Gonen, D. Shi, W. Sheffler, K. K. Fong, U. Nattermann, C. Xu, P. S. Huang, R. Ravichandran, S. Yi, T. N. Davis, T. Gonen, N. P. King, and D. Baker. Design of a hyperstable 60-subunit protein dodecahedron. [corrected]. *Nature*, 535(7610):136–9, 2016.
- [31] Neil P King, William Sheffler, Michael R Sawaya, Breanna S Vollmar, P John, Ingemar André, Tamir Gonen, Todd O Yeates, and David Baker. Computational design of self-assembling protein nanomaterials with atomic level accuracy. *Science*, 336(6085):1171–1174, 2012.
- [32] Quinton M Dowling, Young-jun Park, Neil Gerstenmaier, Erin C Yang, Adam Wargacki, Yang Hsia, and N Chelsea. Hierarchical design of pseudosymmetric protein nanoparticles. *bioRxiv*, 2023.
- [33] A. D. Malay, N. Miyazaki, A. Biela, S. Chakraborti, K. Majsterkiewicz, I. Stupka, C. S. Kaplan, A. Kowalczyk, Bmag Piette, G. K. A. Hochberg, D. Wu, T. P. Wrobel, A. Fineberg, M. S. Kushwah, M. Kelemen, P. Vavpetic, P. Pelicon, P. Kukura, J. L. P. Benesch, K. Iwasaki, and J. G. Heddle. An ultra-stable gold-coordinated protein cage displaying reversible assembly. *Nature*, 569(7756):438–442, 2019.
- [34] H. Ren, S. Zhu, and G. Zheng. Nanoreactor design based on self-assembling protein nanocages. *Int J Mol Sci*, 20(3), 2019. Ren, Huimei Zhu, Shaozhou Zheng, Guojun eng 21706005/National Natural Science Foundation of China Review Switzerland Int J Mol Sci. 2019 Jan 30;20(3). pii: ijms20030592. doi: 10.3390/ijms20030592.
- [35] Joshua Laniado, Kevin A. Cannon, Justin E. Miller, Michael R. Sawaya, Dan E. McNamara, and Todd O. Yeates. Geometric lessons and design strategies for nanoscale protein cages. *ACS Nano*, 15(3):4277–4286, 2021.
- [36] Scott A. McConnell, Kevin A. Cannon, Christian Morgan, Rachel McAllister, Brendan R. Amer, Robert T. Clubb, and Todd O. Yeates. Designed protein cages as scaffolds for building multienzyme materials. *ACS Synthetic Biology*, 9(2):381–391, 2020.
- [37] R. Zandi, D. Reguera, R. F. Bruinsma, W. M. Gelbart, and J. Rudnick. Origin of icosahedral symmetry in viruses. *Proc. Natl. Acad. Sci. U. S. A.*, 101(44):15556–15560, 2004.
- [38] R. Twarock and A. Luque. Structural puzzles in virology solved with an overarching icosahedral design principle. *Nat Commun*, 10(1):4414, 2019.
- [39] Antonio Šiber. Icosadeltahedral geometry of geodesic domes, fullerenes and viruses: A tutorial on the T-number. *Symmetry*, 12(4), 2020.
- [40] J. E. Johnson and J. A. Speir. Quasi-equivalent viruses: A paradigm for protein assemblies. *J. Mol. Biol.*, 269(5):665–675, 1997.
- [41] Donald L. D. Caspar and Annamária Klug. Physical principles in the construction of regular viruses. *Cold Spring Harbor symposia on quantitative biology*, 27:1–24, 1962.
- [42] Siyu Li, Polly Roy, Alex Travasset, and Roya Zandi. Why large icosahedral viruses need scaffolding proteins.

- Proceedings of the National Academy of Sciences of the United States of America*, 115(43):10971–10976, 2018.
- [43] Michael F Hagan and David Chandler. Dynamic pathways for viral capsid assembly. *Biophysical Journal*, 1(91):42–54, 2006.
- [44] Alex W. Wilber, Jonathan P. K. Doye, Ard A. Louis, Eva G. Noya, Mark A. Miller, and Pauline Wong. Reversible self-assembly of patchy particles into monodisperse icosahedral clusters. *The Journal of Chemical Physics*, 127(8):085106, 2007.
- [45] Arunkumar Bupathy, Daan Frenkel, and Srikanth Sastri. Temperature protocols to guide selective self-assembly of competing structures. *PNAS*, 119(8), 2022.
- [46] Maximilian Hübl C. and Carl P Goodrich. Accessing Semi-Addressable Self Assembly with Efficient Structure Enumeration. *arXiv:2405.13567v1*, pages 1–6, 2024.
- [47] Ella M King. Programming patchy particles for materials assembly design. 121(27):1–6, 2024.
- [48] Stephen Whitelam, Carl Rogers, Andrea Pasqua, Chad Paavola, Jonathan Trent, and Phillip L. Geissler. The impact of conformational fluctuations on self-assembly: Cooperative aggregation of archaeal chaperonin proteins. *Nano Letters*, 9:292–297, JAN 2009, 2009.
- [49] Stephen Whitelam and Robert L. Jack. The statistical mechanics of dynamic pathways to self-assembly. *Annual Review of Physical Chemistry*, 66:143–163, 2015.
- [50] Joakim Bohlin, Andrew J. Turberfield, Ard A. Louis, and Petr Šulc. Designing the self-assembly of arbitrary shapes using minimal complexity building blocks. *ACS Nano*, 17(6):5387–5398, 2023. PMID: 36763807.
- [51] Diogo EP Pinto, Petr Šulc, Francesco Sciortino, and John Russo. Design strategies for the self-assembly of polyhedral shells. *Proceedings of the National Academy of Sciences*, 120(16):e2219458120, 2023.
- [52] Diogo E. P. Pinto, Nuno A. M. Araújo, Petr Šulc, and John Russo. Inverse Design of Self-Folding 3D Shells. *Phys. Rev. Lett.*, 118201:1–6, 2024.
- [53] Flavio Romano, John Russo, Luká š Kroc, and Petr Šulc. Designing patchy interactions to self-assemble arbitrary structures. *Phys. Rev. Lett.*, 125:118003, Sep 2020.
- [54] Manuel Mart, Jose M Gomez Llorente, Javier Hern, and David J Wales. Minimal Design Principles for Icosahedral Virus Capsids. *ACS Nano*, 2021.
- [55] Saeed Osat, Jakob Metson, Mehran Kardar, and Ramin Golestanian. Escaping kinetic traps using nonreciprocal interactions. *Phys. Rev. Lett.*, 133:028301, Jul 2024.
- [56] Joshua Evans and Petr Šulc. Designing 3D multi-component self-assembling systems with signal-passing building blocks. *The Journal of Chemical Physics*, 160(8):084902, 02 2024.
- [57] Diogo E. P. Pinto, Petr Šulc, Francesco Sciortino, and John Russo. Automating blueprints for colloidal quasicrystal assembly, 2024.
- [58] Shivendra Pandey, Margaret Ewing, Andrew Kurnas, Nghi Nguyen, David H. Gracias, and Govind Menon. Algorithmic design of self-folding polyhedra. *Proceedings of the National Academy of Sciences*, 108(50):19885–19890, 2011.
- [59] Paul M. Dodd, Pablo F. Damasceno, and Sharon C. Glotzer. Universal folding pathways of polyhedron nets. *Proceedings of the National Academy of Sciences*, 115(29):E6690–E6696, 2018.
- [60] Agnese I. Curatolo, Ofer Kimchi, Carl P. Goodrich, Ryan K. Krueger, and Michael P. Brenner. A computational toolbox for the assembly yield of complex and heterogeneous structures. *Nature Communications*, 14(1):8328, December 2023.
- [61] Sanaz Panahandeh, Siyu Li, Bogdan Dragnea, and Roya Zandi. Virus Assembly Pathways Inside a Host Cell. *ACS Nano*, 2022.
- [62] Sanaz Panahandeh, Siyu Li, Laurent Marichal, Rafael Leite Rubim, Guillaume Tresset, and Roya Zandi. How a Virus Circumvents Energy Barriers to Form Symmetric Shells. *ACS Nano*, 14(3):3170–3180, 2020.
- [63] Jef Wagner and Roya Zandi. The Robust Assembly of Small Symmetric Nanoshells. *Biophysical Journal*, 109(5):956–965, 2015.
- [64] Grant M. Rotskoff and Phillip L. Geissler. Robust nonequilibrium pathways to microcompartment assembly. *Proceedings of the National Academy of Sciences of the United States of America*, 115(25):6341–6346, 2018.
- [65] D. C. Rapaport. Molecular dynamics study of $t = 3$ capsid assembly. *Journal of Biological Physics*, 44(2):147–162, 2018.
- [66] H. D. Nguyen, V. S. Reddy, and C. L. Brooks. Deciphering the Kinetic Mechanism of Spontaneous Self-Assembly of Icosahedral Capsids. *Nano Lett.*, 7(2):338–344, 2007.
- [67] O.M. Elrad and M. F. Hagan. Encapsulation of a polymer by an icosahedral virus. *Phys. Biol.*, 7:045003, 2010.
- [68] Alexander J. Williamson, Alex W. Wilber, Jonathan P. K. Doye, and Ard A. Louis. Templated self-assembly of patchy particles. *Soft Matter*, 7(7):3423–3431, 2011.
- [69] Jason D. Perlmutter, Cong Qiao, and Michael F. Hagan. Viral genome structures are optimal for capsid assembly. *eLife*, 2:e00632, 2013.
- [70] R. Zhang, E. Wernersson, and P. Linse. Icosahedral capsid formation by capsomer subunits and a semiflexible polyion. *RSC Adv.*, 3(47):25258–25267, 2013.
- [71] R. Zhang and P. Linse. Icosahedral capsid formation by capsomers and short polyions. *J. Chem. Phys.*, 138(15), 2013. Zhang, Ran Linse, Per 1089-7690.
- [72] R. Zhang and P. Linse. Topological effects on capsomer-polyion co-assembly. *J. Chem. Phys.*, 140(24), 2014. Zhang, Ran Linse, Per 1089-7690.
- [73] M. Castelnovo, T. Verdier, and L. Foret. Comparing open and closed molecular self-assembly. *Epl-europhys Lett*, 105(2), 2014.
- [74] M. Castelnovo, D. Muriaux, and C. Faivre-Moskalenko. Entropic control of particle sizes during viral self-assembly. *New J. Phys.*, 15, 2013. Castelnovo, M. Muriaux, D. Faivre-Moskalenko, C.
- [75] M. A. Boettcher, H. C. R. Klein, and U. S. Schwarz. Role of dynamic capsomere supply for viral capsid self-assembly. *Phys. Biol.*, 12(1), 2015.
- [76] Carlos I Mendoza and David Reguera. Shape selection and mis-assembly in viral capsid formation by elastic frustration. *eLife*, 9:e52525, 2020.
- [77] R. Schwartz, P. W. Shor, P. E. Prevelige, and B. Berger. Local Rules Simulation of the Kinetics of Virus Capsid Self-Assembly. *Biophys. J.*, 75(6):2626–2636, 1998.
- [78] William M. Jacobs, Aleks Reinhardt, and Daan Frenkel. Rational design of self-assembly pathways for complex multicomponent structures. *Proceedings of the National Academy of Sciences*, 112(20):6313–6318, 2015.
- [79] William M Jacobs and Daan Frenkel. Self-assembly

- protocol design for periodic multicomponent structures. *Soft Matter*, 11(46):8930–8938, 2015.
- [80] William M. Jacobs and Daan Frenkel. Self-assembly of structures with addressable complexity. *Journal of the American Chemical Society*, 138(8):2457–2467, 2016.
- [81] Zorana Zeravcic, Vinothan N Manoharan, and Michael P Brenner. Size limits of self-assembled colloidal structures made using specific interactions. *Proceedings of the National Academy of Sciences*, 111(45):15918–15923, nov 2014.
- [82] Jim Madge and Mark A. Miller. Optimising minimal building blocks for addressable self-assembly. *Soft Matter*, 13:7780–7792, 2017.
- [83] Martin Sajfutdinow, William M. Jacobs, Aleks Reinhardt, Christoph Schneider, and David M. Smith. Direct observation and rational design of nucleation behavior in addressable self-assembly. *Proceedings of the National Academy of Sciences of the United States of America*, 115(26):E5877–E5886, 2018.
- [84] Lester O. Hedges, Ranjan V. Mannige, and Stephen Whitelam. Growth of equilibrium structures built from a large number of distinct component types. *Soft Matter*, 10(34):6404–6416, 2014.
- [85] Stephen Whitelam. Hierarchical assembly may be a way to make large information-rich structures. *Soft Matter*, 11(42):8225–8235, 2015.
- [86] Daichi Hayakawa, Thomas E. Videbæk, Gregory M. Grason, and W. Benjamin Rogers. Symmetry-guided inverse design of self-assembling multiscale dna origami tilings. *ACS Nano*, 18(29):19169–19178, 2024. PMID: 38981100.
- [87] M. Medrano, M. A. Fuertes, A. Valbuena, P. J. Carrillo, A. Rodriguez-Huete, and M. G. Mateu. Imaging and quantitation of a succession of transient intermediates reveal the reversible self-assembly pathway of a simple icosahedral virus capsid. *J Am Chem Soc*, 138(47):15385–15396, 2016. Medrano, Maria Fuertes, Miguel Angel Valbuena, Alejandro Carrillo, Pablo J P Rodriguez-Huete, Alicia Mateu, Mauricio G eng Research Support, Non-U.S. Gov’t 2016/12/10 J Am Chem Soc. 2016 Nov 30;138(47):15385-15396. doi: 10.1021/jacs.6b07663. Epub 2016 Nov 18.
- [88] John H. Conway, Heidi Burgiel, and Chaim Goodman-Strauss. *The Symmetries of Things*. CRC Press Taylor & Francis Group, 2008.
- [89] Sanaz Panahandeh, Siyu Li, and Roya Zandi. The equilibrium structure of self-assembled protein nano-cages. *Nanoscale*, 10(48):22802–22809, 2018.
- [90] Carlos M Duque, Douglas M Hall, Botond Tyukodi, Michael F Hagan, Christian D Santangelo, and Gregory M Grason. Limits of economy and fidelity for programmable assembly of size-controlled triply periodic polyhedra. *PNAS*, 121(18):1–11, 2024.
- [91] Botond Tyukodi, Farzaneh Mohajerani, Douglas M Hall, Gregory M Grason, and Michael F Hagan. Thermodynamic Size Control in Curvature- Frustrated Tubules: Self-Limitation with Open Boundaries. *ACS Nano*, 16(9077-9085), 2022.
- [92] Huang Fang, Botond Tyukodi, W. Benjamin Rogers, and Michael F. Hagan. Polymorphic self-assembly of helical tubules is kinetically controlled. *Soft Matter*, 18(35):6716–6728, 2022.
- [93] Farzaneh Mohajerani, Botond Tyukodi, Christopher J. Schlicksup, Jodi A. Hadden-Perilla, Adam Zlotnick, and Michael F. Hagan. Multiscale Modeling of Hepatitis B Virus Capsid Assembly and Its Dimorphism. *ACS Nano*, 16(9):13845–13859, 2022.
- [94] H. S. Seung and David R. Nelson. Defects in flexible membranes with crystalline order. *Physical Review A*, 38(2):1005–1018, 1988.
- [95] Adam Zlotnick, Jennifer M. Johnson, Paul W. Wingfield, Stephen J. Stahl, and Dan Endres. A theoretical model successfully identifies features of hepatitis B virus capsid assembly. *Biochemistry*, 38(44):14644–14652, 1999.
- [96] Dan Endres and Adam Zlotnick. Model-based analysis of assembly kinetics for virus capsids or other spherical polymers. *Biophysical Journal*, 83(2):1217–1230, 2002.
- [97] Adam Zlotnick. Are weak protein-protein interactions the general rule in capsid assembly? *Virology*, 315(2):269–274, 2003.
- [98] Pablo Ceres and Adam Zlotnick. Weak protein-protein interactions are sufficient to drive assembly of hepatitis B virus capsids. *Biochemistry*, 41(39):11525–11531, 2002.
- [99] Robert L. Jack, Michael F. Hagan, and David Chandler. Fluctuation-dissipation ratios in the dynamics of self-assembly. *Phys. Rev. E*, 76:021119, Aug 2007.
- [100] D.C. Rapaport. The role of reversibility in viral capsid growth: A paradigm for self-assembly. *Physical Review Letters*, 101:186101, 2008.
- [101] Stephen Whitelam, Carl Rogers, Andrea Pasqua, Chad Paavola, Jonathan Trent, and Phillip L. Geissler. The Impact of Conformational Fluctuations on Self-Assembly: Cooperative Aggregation of Archaeal Chaperonin Proteins. *Nano Letters*, 9(1):292–297, January 2009.
- [102] Alex W. Wilber, Jonathan P. K. Doye, Ard A. Louis, and Anna C. F. Lewis. Monodisperse self-assembly in a model with protein-like interactions. *Journal of Chemical Physics*, 131(17):175102, 2009.
- [103] M. F. Hagan, O. M. Elrad, and R. L. Jack. Mechanisms of kinetic trapping in self-assembly and phase transformation. *Journal of Chemical Physics*, 135:104115, 2011.
- [104] Shengfeng Cheng, Ankush Aggarwal, and Mark J. Stevens. Self-assembly of artificial microtubules. *Soft Matter*, 8(20):5666, 2012.
- [105] Michael F Hagan. Modeling Viral Capsid Assembly. *Adv. Chem. Phys.*, 155:1–68, 2014.
- [106] Jason D Perlmutter, Farzaneh Mohajerani, and Michael F Hagan. Many-molecule encapsulation by an icosahedral shell. *eLife*, 5:e14078, may 2016.
- [107] Roi Asor, Christopher John Schlicksup, Zhongchao Zhao, Adam Zlotnick, and Uri Raviv. Rapidly forming early intermediate structures dictate the pathway of capsid assembly. *Journal of the American Chemical Society*, 142(17):7868–7882, 2020. PMID: 32233479.
- [108] Yian Qian, Daniel Evans, Bhavya Mishra, Yiben Fu, Zixiu Hugh Liu, Sikao Guo, and Margaret E. Johnson. Temporal control by cofactors prevents kinetic trapping in retroviral Gag lattice assembly. *Biophysical Journal*, 122(15):3173–3190, August 2023.